Advanced Powder Technology 31 (2020) 1023–1031

Contents lists available at ScienceDirect

Advanced Powder Technology

journal homepage: www.elsevier.com/locate/apt

Original Research Paper

Effects of metal oxide nanoparticles on combustion and gas-generating performance of NaN_3/Al composite powders ignited using a microhotplate platform

Ho Sung Kim [a,1], Ji Hoon Kim [a,1], Ji Hye Ku [a], Myung Hoon Cho [a], Jung Keun Cha [a], Jong Man Kim [a,b], Hyung Woo Lee [a,b], Soo Hyung Kim [a,b,*]

[a] Department of Nano Fusion Technology, College of Nanoscience and Nanotechnology, Pusan National University, 30 Jangjeon-dong, Geumjung-gu, Busan 609-735, Republic of Korea
[b] Department of Nano Energy Engineering, College of Nanoscience and Nanotechnology, Pusan National University, 30 Jangjeon-dong, Geumjung-gu, Busan 609-735, Republic of Korea

ARTICLE INFO

Article history:
Received 8 June 2019
Received in revised form 15 December 2019
Accepted 24 December 2019
Available online 7 January 2020

Keywords:
Al nanoparticle
Oxidizer
Sodium azide microparticle
Microhotplate heater
Gas generator

ABSTRACT

We investigated the effects of different metal oxide (MO) nanoparticles (e.g., CuO, KIO_4, Fe_2O_3) on the combustion and gas-generating characteristics of sodium azide microparticle (NaN_3 MP; gas-generating agent) and aluminum nanoparticle (Al NP; heat source) composite powders. The NaN_3 MP/Al NP/MO NP composite powders were stably ignited using a microhotplate (MHP) heater. The addition of CuO and KIO_4 to the NaN_3 MP/Al NP composite powders resulted in relatively high burn rates and high pressurization rates upon MHP-assisted ignition. This suggests that the highly reactive CuO and KIO_4 NPs significantly increased the combustion of the Al NPs; as a result, sufficient heat energy was generated via the active aluminothermic reaction to thermally decompose the NaN_3 MPs. Finally, the gas generating properties of NaN_3 MP/Al NP composite powders mixed with various MO NPs were tested using home-made inflatable small airbags. The airbags were fully inflated within ~20 ms when CuO and KIO_4 NPs were added to the NaN_3 MP/Al NP composite powders. However, the addition of Fe_2O_3 NPs to the NaN_3 MP/Al NP composite powder resulted in a slow and only partial inflation of the airbag due to an incomplete aluminothermic reaction, which was due to a slow combustion reaction between the Al NPs and relatively weak oxidizer of the Fe_2O_3 NPs. This suggests that the rapid, stable, and complete thermal decomposition of NaN_3 MP/Al NP composites can be effectively achieved by employing highly reactive nanoscale oxidizers.

1. Introduction

An energetic material (EM) is any substance composed of a fuel and an oxidizing agent that rapidly converts chemical energy into thermal energy when ignited via an external energy input [1–3]. Nanoscale energetic materials (nEMs), in particular, have the advantages of relatively high heat energy release rates and improved combustion properties [4–6]. In the various nEM formulations, nanosized Al is most widely used as a fuel material and various nanosized metal oxides (MOs) such as Fe_2O_3, MoO_3, $KMnO_4$, CuO, NiO, MnO_2, and WO_3 are used as oxidizers [7–12].

nEMs are activated as the critical temperature is reached. Once they are activated, thermal reactions such as combustion and explosions can occur. Therefore, it is important to control the ignition and combustion reactions of nEMs not only for safety while handling them, but also for diversifying their applications [13–15]. Various heat sources such as electric sparks, flames, flashes, and lasers have been used as external energy sources to safely ignite nEMs. The micro-electro-mechanical system (MEMS) technology-based microhotplate (MHP) heater is one of the various systems that has been employed for ignition. It has the advantages of easy miniaturization, temperature controllability, and diversification of ignition spots [16–18].

A gas generator generates large amounts of gas via a chemical reaction between a fuel and oxidizer. It is used in instances when storing a pressurized gas is undesirable [19–21], and it is suitable for the rapid inflation of airbags. Gas-generating materials have to meet several requirements, including good performance

* Corresponding author at: Department of Nano Fusion Technology, College of Nanoscience and Nanotechnology, Pusan National University, 30 Jangjeon-dong, Geumjung-gu, Busan 609-735, Republic of Korea.
E-mail address: sookim@pusan.ac.kr (S.H. Kim).
[1] Both H.S. Kim and J.H. Kim equally contributed to this work as the first authors.

https://doi.org/10.1016/j.apt.2019.12.034
0921-8831/

reproducibility, easy and reliable ignition, low explosion temperature/heat/condensed products, and high specific energy and gas generation capabilities. The gas-generating materials in gas generators thermally decompose into gases and residual composite materials when they are ignited. Previous gas generators used for the production of nitrogen gas employed various nitrogen compounds, including sodium azide (NaN_3), triazole ($C_2H_3N_3$), and guanidine nitrate ($CH_6N_4O_3$), as the primary source of gas in addition to various MOs [22–29]. When a vehicle collides with something, the gas-generating materials are activated and they begin to thermally decompose, producing nitrogen gas and various residual compounds. However, incomplete combustion reactions frequently occur in gas generators because of insufficient heat energy. Various studies have been performed using metals (e.g., Al, Mg) and metal nitrates (e.g., $Cu(NO_3)_2$, $Sr(NO_3)_2$) as additional heat energy sources to achieve complete thermochemical combustion between the reacting EMs [30–32].

Herein, we examine the effects of MOs on the gas-generating performance of NaN_3 and Al composite powders. Specifically, NaN_3 microparticles (MPs) are used as gas-generating materials, highly reactive Al nanoparticles (NPs) are used as a fuel, and various MOs, including CuO, Fe_2O_3, and KIO_4, are used as oxidizing agents. The combustion and gas-generating characteristics of the NaN_3 MP/Al NP composite powders are observed by varying the type of oxidizer NPs before ignition. The composite powders were ignited using a specially designed MHP heater manufactured using MEMS technology. The MHP heater was also used with an airbag system to observe the gas-generating and airbag inflating performance of the powders.

2. Experimental

2.1. Material fabrication

The MHP heater was fabricated via a metal lift-off process, as illustrated in Fig. 1a. An ~1.4-μm-thick photoresist mold (PR; AZ5214, Clariant) was formed on an oxidized silicon substrate through a standard image reversal (IR) photolithography process. The IR process is useful for producing negatively sloped sidewalls in a PR mold, which makes the subsequent lift-off process easier. The PR was spin-coated on the oxidized silicon substrate at 4000 rpm for 35 s and soft-baked on a hotplate at 95 °C for 5 min. The PR layer was then exposed to ultraviolet (UV) radiation with an intensity of ~20 mW/cm^2 through a photomask using a commercially available mask aligning system (MDA-400M, Midas System). The UV-exposed region of the PR layer was cross-linked by further baking it on a hot plate at 115 °C for 2.5 min. Subsequently, the processed PR layer was fully exposed to UV radiation without a photomask to solubilize the non-cross-linked region. Finally, the PR mold patterns were produced by dissolving the noncross-linked region using a developer (AZ300 MIF, Clariant). An ~150-nm-thick Au layer was then deposited on the prepared mold substrate containing a Cr adhesion layer (~10-nm thick) using a thermal evaporation technique. Finally, serpentine-shaped MHP patterns were defined by selectively removing the unnecessary portions of the deposited Au thin film in an ultrasonic bath containing acetone.

NaN_3 MPs (average diameter ($\bar{D_p}$) = ~80 μm, Sigma-Aldrich) and Al NPs (NT Base Inc.) were used as the gas-generating and fuel materials, respectively, without further treatment. Commercially available CuO NPs (NT Base Inc.) and Fe_2O_3 NPs (Sigma-Aldrich) were used as oxidizers. The KIO_4 NPs were fabricated using a spray pyrolysis method [33–35]. Specifically, 0.4 g of KIO_4 (Sigma-Aldrich) was dissolved in 100 ml of deionized water. Aerosol droplets containing the KIO_4 precursor were generated using a standard atomizer operated using compressed air at 35 psi. The aerosol droplets were then passed through a silica-gel dryer followed by a tube furnace heated at 180 °C. The KIO_4 NPs were finally collected using a membrane filter with 200 nm pores. Fig. 1b shows a schematic of the fabrication of the NaN_3 MP/Al NP/MO NP composite powders. Three different composite powders of NaN_3 MP/Al NP/CuO NP, NaN_3 MP/Al NP/Fe_2O_3 NP, and NaN_3 MP/Al NP/KIO_4 NP were fabricated using simple sonication and drying processes. The mixing ratio for the composite powder was fixed as NaN_3:Al:MO = 77:7:16 wt%. The resulting fuel-to-oxidizer ratio in the composites was calculated to be ~1.90 for Al/CuO, ~1.27 for Al/Fe_2O_3, and ~1.37 for Al/KIO_4, respectively. This ratio enabled the composite powders to be stably ignited and to actively generate gaseous byproducts. It is noted that applying different amount of fuel and oxidizer could strongly affect the evolution rate of heat and pressure and eventually gas production rate. Specifically, each reactant was mixed in an ethanol solution for 30 min via ultrasonication at 170 W and 40 kHz. These prepared samples were then dried in a convection oven for 30 min at 80 °C to prepare the NaN_3/Al/MO composite powders. They were then deposited on the surface of the MHP for realizing gas generators. When a specific voltage was supplied to the MHP, a resistance heat was generated and the composite powders were ignited.

2.2. Combustion and explosion characterization of NaN_3/Al/MO composite powders

The burn rate and total burning time of the NaN_3/Al/MO composite powders were measured using a high-speed camera (Model FASTCAM SA3 120 K, Photron) at a frame rate of 5 kHz. The high-speed camera had a 17.4 mm × 17.4 mm CMOS image sensor with a minimum and maximum frame rate of 60 and 1,200,000 fps, respectively, and a pixel size of 17 μm × 17 μm, with an operating voltage and current of AC 100–240 V and 60 A, respectively.

The pressure traces of the ignited composite powders as a function of time were measured using a pressure cell tester (PCT) system. The PCT consisted of a pressure cell with constant volume of 13 ml, pressure sensor (Model 480C02, PCB Piezotronics), signal conditioner (Model 480C02, PCB Piezotronics), signal amplifier (Model 422E11, PCB Piezotronics), oscilloscope (Tektronix, Model TDS 2012B), and power supply. Approximately 13 mg of composite powder was spin-coated on the surface of the MHP installed inside the pressure cell. The powder was then ignited by the MHP-generated heat energy and the pressure was automatically measured using the pressure sensor connected to the pressure cell. Simultaneously, the detected pressure signal was amplified and transformed into a voltage signal using a combination of an in-line charge amplifier and a signal conditioner. Finally, the converted electrical signal was detected and recorded using a digital oscilloscope.

2.3. Material characterization

The fabricated NaN_3/Al/MO composite powders were characterized using various techniques, including field emission scanning electron microscopy (FE-SEM; Model S4700, Hitachi, Ltd.) performed at ~15 kV, scanning transmission electron microscopy (S-TEM; Model JEM-2100, JEOL, Ltd.) performed at ~200 kV, X-ray diffractometry (XRD; Model Empyrean Series 2, PANalytical, Ltd.) using Cu Kα radiation, and differential scanning calorimetry (DSC; Model Labsys TGA-DSC/DTA evo, Setaram, Ltd.) performed at temperatures ranging from 30 to 1000 °C at a heating rate of 10 °C/min under N_2 flow.

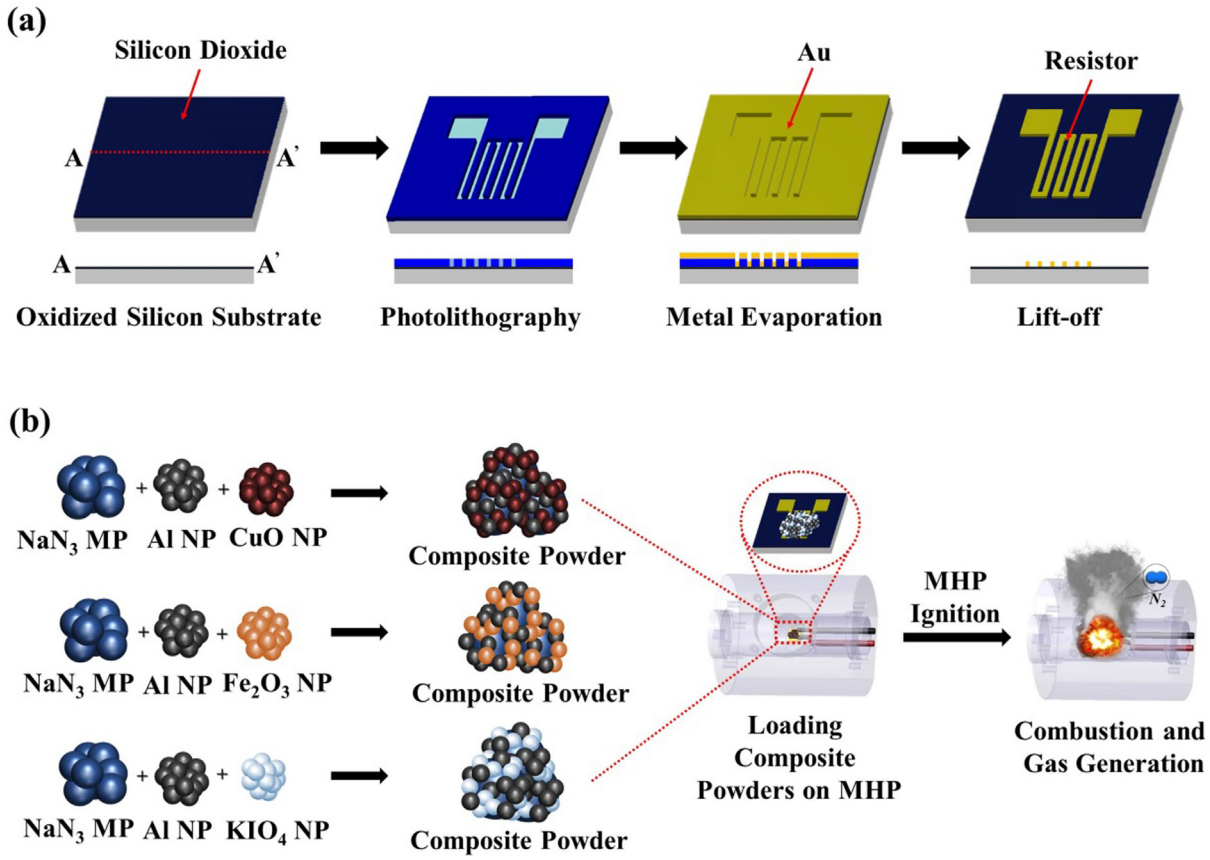

Fig. 1. (a) Schematic of MEMS-based processes for fabricating microhotplates (MHPs), and (b) schematic of fabrication and MHP-assisted ignition of NaN_3 MP/Al NP/CuO NP, NaN_3 MP/Al NP/Fe_2O_3 NP, NaN_3 MP/Al NP/KIO_4 NP composite powders.

3. Results and discussion

Fig. 2 shows the SEM and EDX images of three different NaN_3/Al/MO composite powders. Fig. 2a and b present the SEM and EDX images of the NaN_3 MP/Al NP/CuO NP composite powders, in which spherical Al and CuO NPs were bound to the surface of NaN_3 MPs with an average diameter of ~80 μm. Fig. 2c and d present the SEM and EDX images of the NaN_3 MP/Al NP/Fe_2O_3 NP composite powder, in which spherical Al and Fe_2O_3 NPs were bound to the surface of NaN_3 MPs. Fig. 2e and f present the SEM and EDX images of the NaN_3 MP/Al NP/KIO_4 NP composite powder, in which spherical Al and KIO_4 NPs were bound to the surface of NaN_3 MPs.

TEM and STEM analyses were performed to observe fuel and oxidizer NPs. Fig. 3 shows that Al NPs and various MO NPs (i.e., CuO, Fe_2O_3, and KIO_4) with spherical shapes were bonded to each other at the nanoscale due to Van der Waals attraction forces. The average sizes of the Al NP/CuO NP, Al NP/Fe_2O_3 NP, and Al NP/KIO_4 NP were ~158 ± 11.4 nm, ~43 ± 1.2 nm, and ~59 ± 1.4 n m, respectively.

A series of MHP-assisted ignition tests were performed to evaluate the effect of MO on the combustion and explosion of NaN_3/Al composites. Fig. 4 shows the sequential still images of MHP-assisted ignition and flame propagation of NaN_3/Al/MO composite powders observed using a high-speed camera. It is noted that the first still images were set to 0 ms just before the ignition of each composite, and then the following still images were arranged by time elapsed after the ignition of each composite. All three composite powders were successfully ignited via MHP initiation. The process started with localized ignition and the flame generated was then propagated to the adjacent composite powders in series. The resulting burn rates of the composite powders due to MHP ignition were experimentally determined to be ~60 ± 3.6 m/s for NaN_3 MP/Al NP/CuO NP, ~6.3 ± 0.5 m/s for NaN_3 MP/Al NP/KIO_4 NP, and ~3.8 ± 0.3 m/s for NaN_3 MP/Al NP/Fe_2O_3 NP. The burn rate of the composite powders was determined as the total length (10 mm) of the aligned powder sample divided by the total time necessary for the flame generated during ignition to propagate from one end to the other of the powder sample. The total burning time of the NaN_3 MP/Al NP/CuO NP, NaN_3 MP/Al NP/KIO_4 NP and NaN_3 MP/Al NP/Fe_2O_3 NP composite powders via MHP ignition was found to be ~8.3 ± 0.4 ms, ~41.3 ± 2.5 ms and ~62.3 ± 3.4 ms, respectively. The total burning time was calculated as the time from the beginning of ignition to the end of the burning process. The most effective oxygen providers for the self-propagating combustion of the NaN_3 MP/Al NP composite powders were as follows: CuO NPs > KIO_4 NPs > Fe_2O_3 NPs.

DSC analyses were performed to investigate the effect of MO on the thermal properties of the NaN_3/Al composite powders. Fig. 5 shows the results of the DSC analyses, in which the effect of MO on the total heat energy generated by the exothermic reaction of NaN_3/Al was examined. The exothermic reactions for NaN_3 MP/Al NP/CuO NP, NaN_3 MP/Al NP/KIO_4 NP, and NaN_3 MP/Al NP/Fe_2O_3 NP composite powders were initiated at ~380 °C, ~390 °C, and ~410 °C, respectively. In general, NaN_3 thermally decomposes at 350–400 °C [36,37], and the exothermic reactions for the Al NP/CuO NP, Al NP/KIO_4 NP, and Al NP/Fe_2O_3 NP powders occur at 450–600 °C [12,32]. However, the NaN_3/Al/MO composite powders began to generate heat energy at lower initiation t-

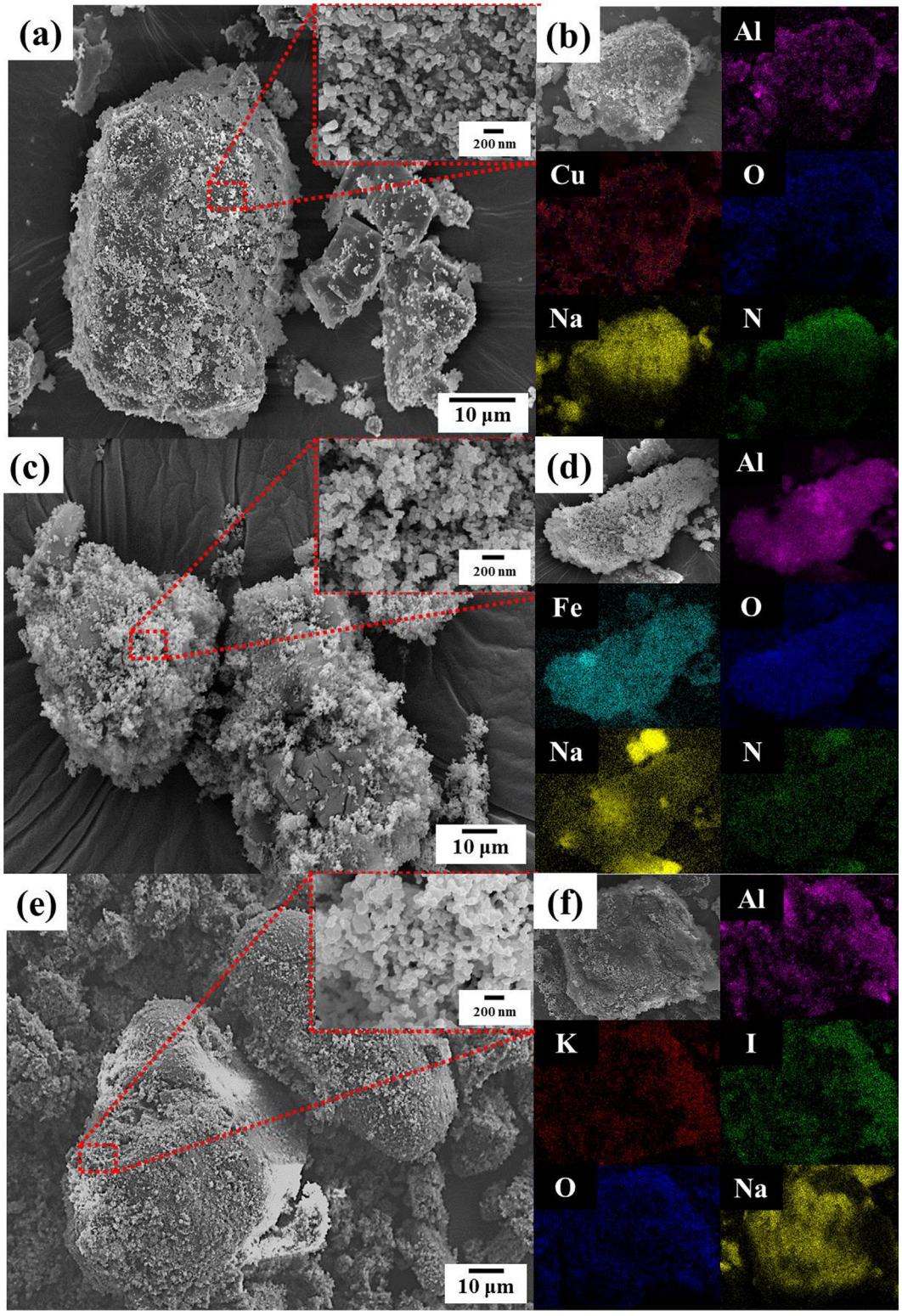

Fig. 2. SEM and EDX images of (a, b) NaN_3 MP/Al NP/CuO NP, (c, d) NaN_3 MP/Al NP/Fe_2O_3 NP, (e, f) NaN_3 MP/Al NP/KIO_4 NP composite powders.

emperatures of 380–410 °C. This suggests that the exothermic reactions of Al NP/MO NP were initiated by the heat energy generated by the thermal decomposition of NaN_3 MPs. By integrating the exothermic curves, the amount of total heat energy released during the thermite reaction in the composite powders was determined to be ~3214 J/g for NaN_3 MP/Al NP/CuO NP, ~2307 J/g for NaN_3 MP/Al NP/KIO_4 NP, and ~683 J/g for NaN_3 MP/Al NP/Fe_2O_3 NP. This suggests that the most effective oxygen providers were as follows: CuO > KIO_4 > Fe_2O_3; hence, the thermal reactions occurred accordingly.

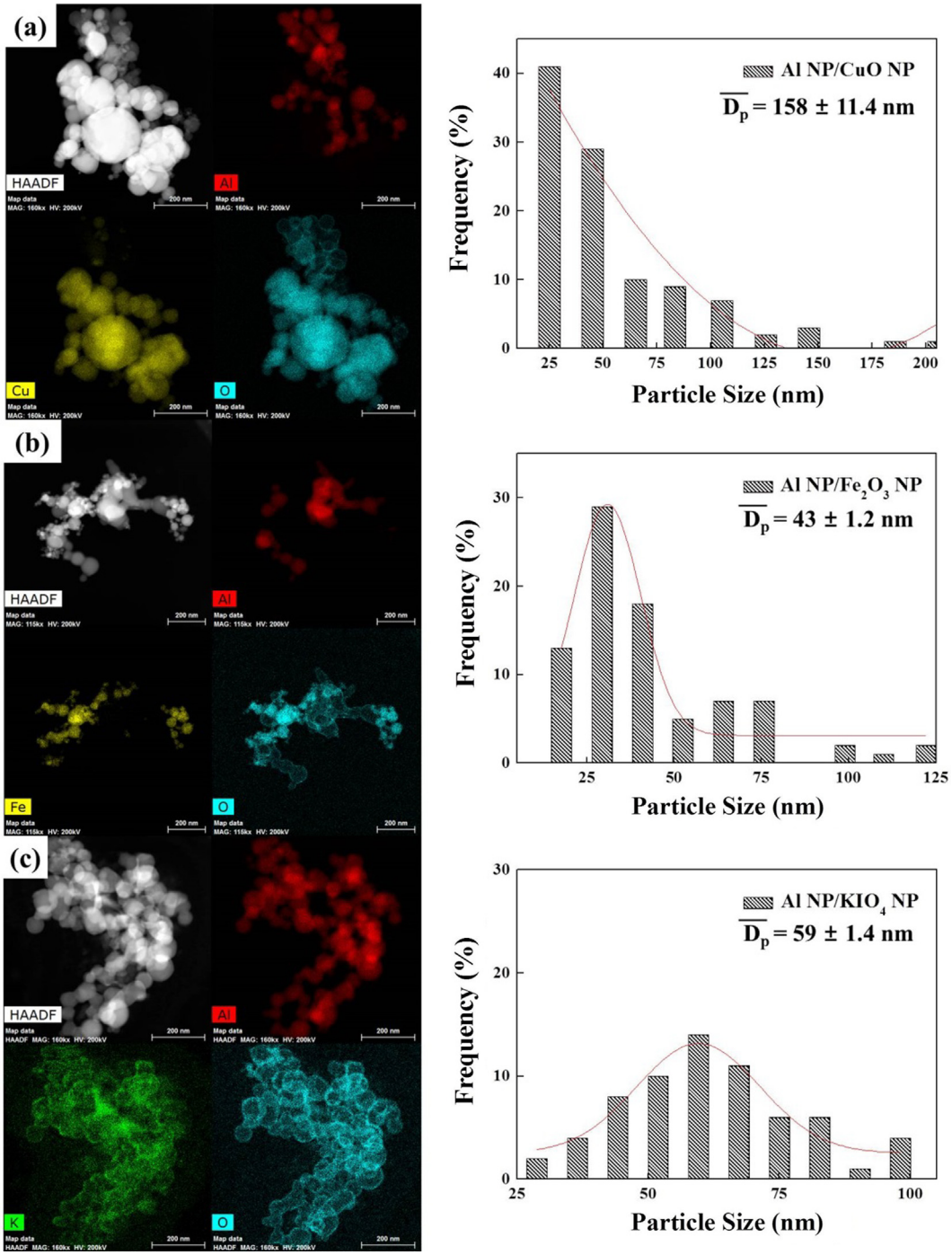

Fig. 3. TEM/STEM images and particle size distributions of (a) NaN_3 MP/Al NP/CuO NP, (b) NaN_3 MP/Al NP/Fe_2O_3 NP, and (c) NaN_3 MP/Al NP/KIO_4 NP composite powders.

XRD measurements were performed before and after the combustion reactions of the composite powders to examine the reactants and products of the three composite powders, as shown in Fig. 6. In the case of the NaN_3 MP/Al NP/CuO NP composite powder, strong peaks from NaN_3, CuO and Al were observed before combustion (Fig. 6a). After the thermochemical reactions of the NaN_3/Al/CuO reactants, various products can be expected to be generated as follows [38,39]:

$$2NaN_3 \rightarrow 2Na + 3N_2$$

$$2Al + 3CuO \rightarrow Al_2O_3 + 3Cu$$

$$2Na + CuO \rightarrow Na_2O + Cu$$

Strong indicators of Na_2O, Al_2O_3, and Cu were clearly observed after the combustion of NaN_3 MP/Al NP/CuO NP composite powder (Fig. 6a). In the case of NaN_3 MP/Al NP/KIO_4 NP composite powders, various products can be formed as follows [40,41]:

$$2NaN_3 \rightarrow 2Na + 3N_2$$

$$8Al + 3KIO_4 \rightarrow 4Al_2O_3 + 3KI$$

$$8Na + KIO_4 \rightarrow 4Na_2O + KI$$

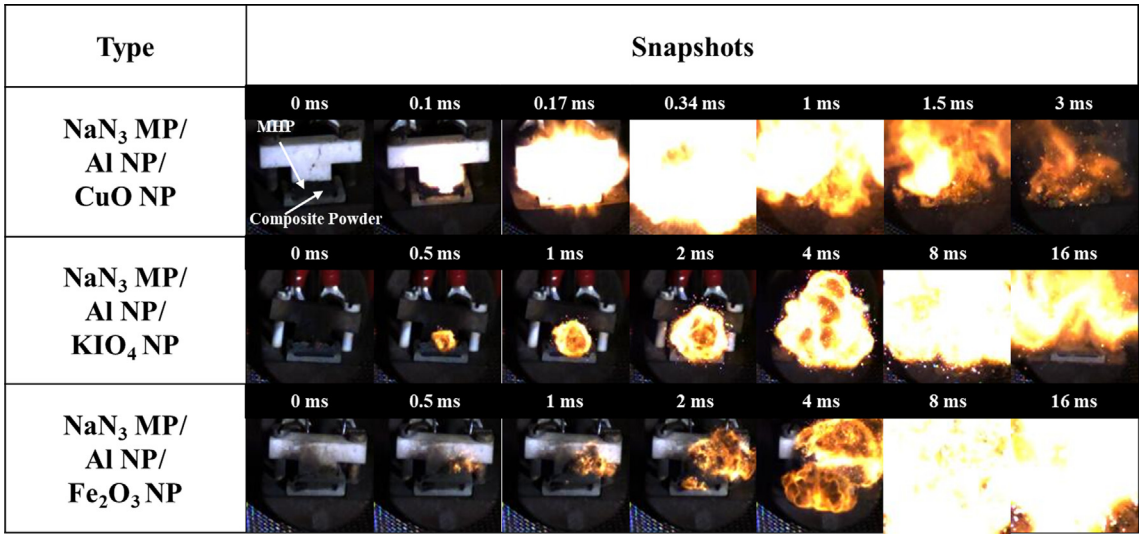

Fig. 4. Snapshots of MHP-assisted ignition and combustion of NaN_3 MP/Al NP/CuO NP, NaN_3 MP/Al NP/KIO_4 NP, and NaN_3 MP/Al NP/Fe_2O_3 composite powders.

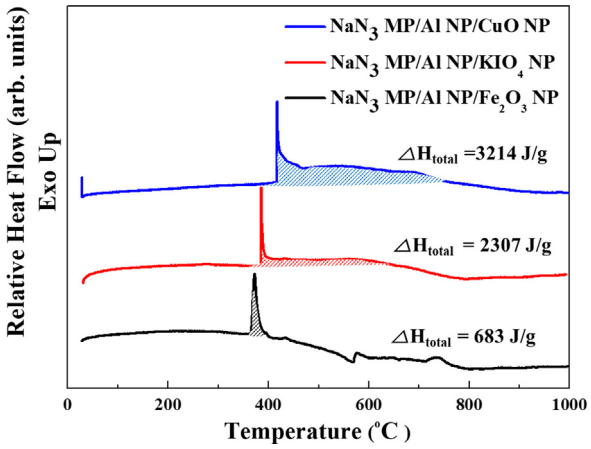

Fig. 5. Differential scanning calorimetry (DSC) results of NaN_3 MP/Al NP/CuO NP, NaN_3 MP/Al NP/KIO_4 NP, and NaN_3 MP/Al NP/Fe_2O_3 NP composite powders.

We observed that Na, KI, Na_2O, and Al_2O_3 phases were clearly formed. However, peaks indicating unreacted NaN_3 were also observed, as shown in Fig. 6b.

$$2NaN_3 \rightarrow 2Na + 3N_2$$

$$2Al + Fe_2O_3 \rightarrow Al_2O_3 + 2Fe_2O_3$$

$$2Na + Fe_2O_3 \rightarrow Na_2O + 2Fe$$

In the case of the NaN_3 MP/Al NP/Fe_2O_3 NP composite powders, Fe, Na_2O, and Al_2O_3 were expected to be formed after the combustion reaction, but the reactants of Al, Fe_2O_3, and NaN_3 remained unreacted, as shown in Fig. 6c. This suggests that the NaN_3/Al composite with CuO NPs thermochemically reacted in the combustion process under sufficient exothermic heat energy, while the NaN_3/Al composite with KIO_4 and Fe_2O_3 partially reacted due to lack of sufficient heat energy; thus, unreacted chemicals remained even after the combustion processes.

The three composite powders were ignited in a pressure cell in which the pressure traces were measured. As shown in Fig. 7a, the maximum pressure generated by the combustion reaction was in the following order: NaN_3 MP/Al NP/CuO NP > NaN_3 MP/Al NP/KIO_4 NP > NaN_3 MP/Al NP/Fe_2O_3 NP. This was mainly due to volume expansion triggered by the thermal decomposition of NaN_3 MPs. This suggests that the thermal decomposition of NaN_3 MPs was effectively made due to the oxidizers containing CuO and KIO_4 rather than Fe_2O_3. Fig. 7b shows the pressurization rate, which is determined by calculating the ratio of the maximum pressure to the rise time. Steeper slopes in the time-pressure graphs indicate higher pressurization rates. The addition of CuO or KIO_4 NPs in the NaN_3 MP/Al NP matrix composite powder resulted in a higher pressurization rates, suggesting that rapid thermal decomposition of NaN_3 was effectively achieved owing to the presence of strong oxidizers of CuO and KIO_4.

The actual amount of gas generated for the three different composite powders was experimentally determined via a water substitution method. The experimental data for the volume of N_2 gas generated as a function of the NaN_3 mass in the composites were compared with theoretically determined values, as shown in Fig. 8. The gas generator was first sealed and an MHP was used to ignite the three composite powders in the gas generator. As the amount of NaN_3 increased in the composite powders, the volume of generated N_2 gas increased linearly with the addition of MO to the NaN_3/Al matrix. The actual volume of N_2 gas generated from the NaN_3 MP/Al NP/Fe_2O_3 NP composite powder was much lower than the theoretical values, because the process of thermal decomposition of the NaN_3 MPs was incomplete. However, there was a clear increase in the volume of N_2 gas with the addition of CuO and KIO_4 NPs to the NaN_3/Al matrix, suggesting that the ignition and combustion of the Al NP/CuO NP and Al NP/KIO_4 NP composite provided more heat energy to promote the thermal decomposition of the NaN_3 MPs.

The potential application of gas generators with NaN_3 MP/Al NP/CuO NP, NaN_3 MP/Al NP/KIO_4 NP, and NaN_3 MP/Al NP/Fe_2O_3 NP composite powders was tested for the inflation of small airbags, as shown in Fig. 9a. The three different composite powders were ignited using an MHP in the gas generator and the airbags expanded owing to the gaseous products of the combustion reactions of the composites. Fig. 9b shows snapshots of the airbag expansion for the three tested composite powders. The small airbags were made of rubber-coated cloth to prevent gas leakage and the total volume of the small airbag was ~150 ml. The amount of NaN_3 MPs added to the composite powders was fixed at ~308 mg, which was theoretically expected to generate ~159 ml of N_2 gas to fully inflate the small airbag. The airbags with the NaN_3

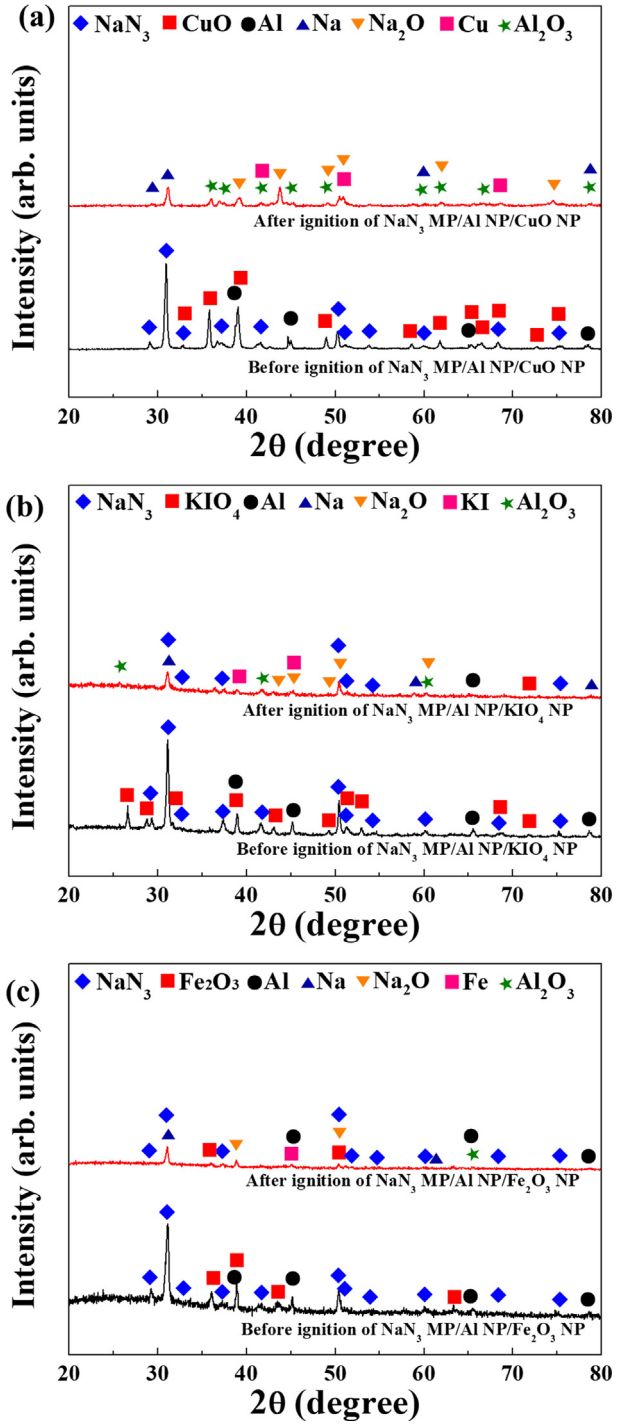

Fig. 6. XRD analyses of (a) NaN_3 MP/Al NP/CuO NP, (b) NaN_3 MP/Al NP/KIO_4 NP, and (c) NaN_3 MP/Al NP/Fe_2O_3 NP composite powders before and after thermal ignition and subsequent combustion reaction.

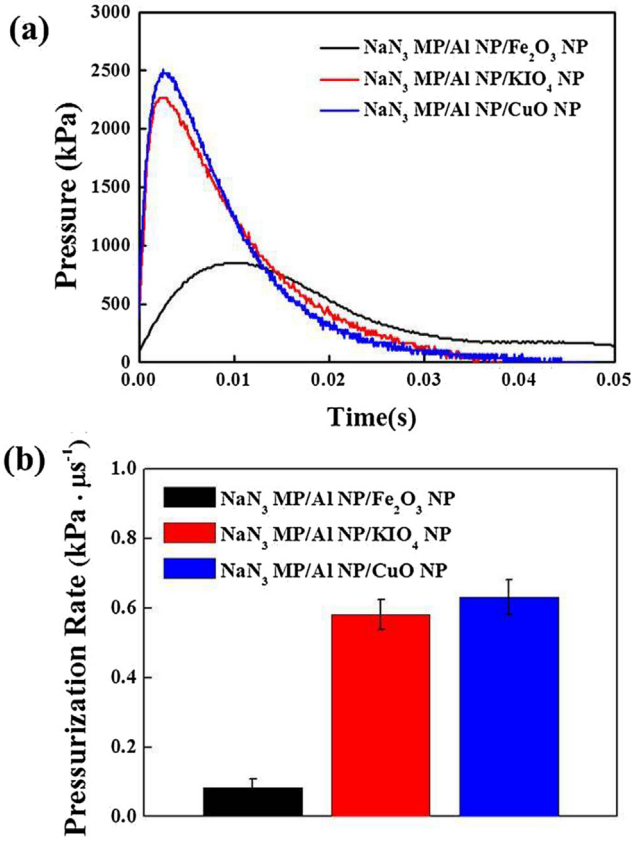

Fig. 7. Comparison of (a) pressure traces and (b) pressurization rates of NaN_3 MP/Al NP/CuO NP, NaN_3 MP/Al NP/KIO_4 NP, and NaN_3 MP/Al NP/Fe_2O_3 NP composite powders loaded in the constant volume of 13 ml reaction vessel in the pressure cell.

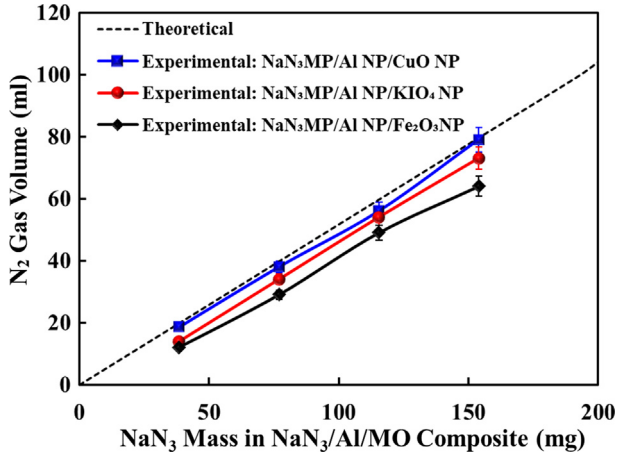

Fig. 8. Comparison of theoretical N_2 gas volume generated with experimentally determined N_2 gas volume generated by ignition and combustion reaction of NaN_3 MP/Al NP/CuO NP, NaN_3 MP/Al NP/KIO_4 NP, and NaN_3 MP/Al NP/Fe_2O_3 NP composite powders.

MP/Al NP/CuO NP and NaN_3 MP/Al NP/KIO_4 NP composite powders took ~10 ms and ~16.7 ms to fully expand. However, the airbag with the NaN_3 MP/Al NP/Fe_2O_3 NP composite powder did not fully inflate even after ~20 ms. Gas generators with CuO and KIO_4-added NaN_3/Al matrices achieved complete airbag expansion because a sufficient amount of N_2 gas was generated by the combustion of the reactants. Full airbag expansion was only achieved for the CuO and KIO_4-added NaN_3 MP/Al NP composite within ~20 ms, suggesting that the required volume of N_2 gas was rapidly generated by the thermal decomposition of NaN_3 in addition to the heat energy generated by the strong aluminothermic reaction between Al NPs and strong oxidizers of CuO and KIO_4 NPs. This confirms that CuO and KIO_4 are more effective than Fe_2O_3 for gas generation by decomposing NaN_3 in the gas generator.

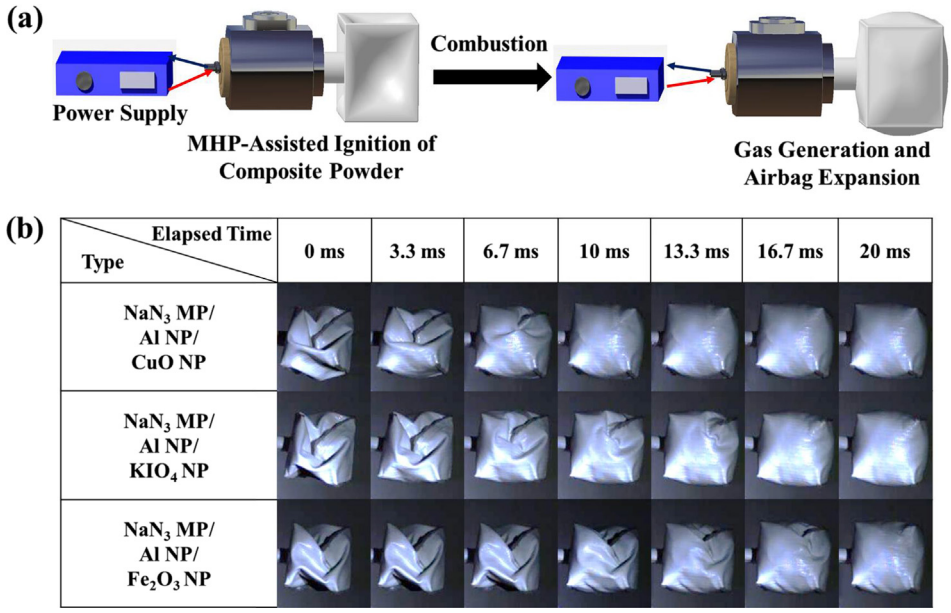

Fig. 9. (a) Schematic of gas generator and small airbag inflation system, and (b) snapshots of small airbags with total volume of 150 ml inflated by MHP ignition and subsequent combustion reaction of NaN_3 MP/Al NP/CuO NP composite powder (full inflation), NaN_3 MP/Al NP/KIO_4 NP composite powder (full inflation), and NaN_3 MP/Al NP/Fe_2O_3 NP composite powder (partial inflation).

4. Conclusions

We investigated the effects of various oxidizing agents of CuO, KIO_4, and Fe_2O_3 NPs on the combustion and gas-generating performance of NaN_3 MP and Al NP composite powders. The NaN_3/Al/MO composite powders were ignited using MHPs, which can be used for miniaturized and versatile gas generators. Among the various composites tested, CuO and KIO_4 NP-added NaN_3 MP/Al NP composite powders released relatively high exothermic energy and had rapid gas-generating properties in the ignition and combustion reactions. This suggests that the use of highly reactive CuO and KIO_4 NPs as strong oxidizers will result in a significant increase in the combustion reaction of Al NPs; as a result, the active aluminothermic reaction occurs to provide heat energy for thermally decomposing the NaN_3 MPs as a gas-generating material. Finally, the NaN_3 MP/Al NP composite powders were successfully demonstrated to fully inflate a small airbag in less than ~20 ms by employing CuO and KIO_4 NPs. However, when Fe_2O_3 NPs were added to the NaN_3/Al matrix, the small airbag was inflated very slowly and only partially owing to the incomplete aluminothermic reaction of the Al NPs generated by the relatively weak oxidizer of the Fe_2O_3 NPs. This suggests that rapid, stable, and complete thermal decomposition of NaN_3 MP/Al NP composites can be effectively achieved by employing highly reactive nanoscale oxidizers.

Acknowledgements

This study was supported by a 2-Year Research Grant of Pusan National University, South Korea.

References

[1] S.H. Kim, M.R. Zachariah, Enhancing the rate of energy release from nanoenergetic materials by electrostatically enhanced assembly, Adv. Mater. 16 (20) (2004) 1821–1825.
[2] J.Y. Ahn, S.H. Kim, Encapsulation of aluminum nanoparticles with copper oxide matrix for enhancing their reactive properties, Chem. Eng. J. 325 (2017) 249–256.
[3] V.E. Sanders, B.W. Asay, T.J. Foley, B.C. Tappan, A.N. Pacheco, S.F. Son, Reaction propagation of four nanoscale energetic composites (Al/MoO_3, Al/WO_3, Al/CuO, and $B1_2O_3$), J. Propul. Power 23 (4) (2007) 707–714.
[4] J.H. Kim, S.B. Kim, M.G. Choi, D.H. Kim, K.T. Kim, H.M. Lee, S.H. Kim, Flash-ignitable nanoenergetic materials with tunable underwater explosion reactivity: The role of sea urchin-like carbon nanotubes, Combust. Flame 162 (4) (2015) 1448–1454.
[5] J.H. Kim, J.Y. Ahn, H.S. Park, S.H. Kim, Optical ignition of nanoenergetic materials: the role of single-walled carbon nanotubes as potential optical igniters, Combust. Flame 160 (4) (2013) 830–834.
[6] M.R. Manaa, A.R. Mitchell, R.G. Garza, P.F. Pagoria, B.E. Watkins, Flash ignition and initiation of explosives–nanotubes mixture, J. Am. Chem. Soc. 127 (40) (2005) 13786–13787.
[7] J.Y. Ahn, W.D. Kim, K. Cho, D. Lee, S.H. Kim, Effect of metal oxide nanostructures on the explosive property of metastable intermolecular composite particles, Powder Technol. 211 (1) (2011) 65–71.
[8] P. Sai Karthik, S.B. Chandrasekhar, D. Chakravarty, D. Srinivas, V.S.K. Chakravadhanula, T.N. Rao, Propellant grade ultrafine aluminum powder by RF induction plasma, Adv. Powder Technol. 29 (3) (2018) 804–812.
[9] H. Liu, J. Zhang, J. Gou, Y. Sun, Preparation of Fe_2O_3/Al composite powders by homogeneous precipitation method, Adv. Powder Technol. 28 (12) (2017) 3241–3246.
[10] K.B. Plantier, M.L. Pantoya, A.E. Gash, Combustion wave speeds of nanocomposite Al/Fe_2O_3: the effects of Fe_2O_3 particle synthesis technique, Combust. Flame 140 (4) (2005) 299–309.
[11] N. Zhao, C. He, J. Liu, H. Gong, T. An, H. Xu, F. Zhao, R. Hu, H. Ma, J. Zhang, Dependence of catalytic properties of Al/Fe_2O_3 thermites on morphology of Fe_2O_3 particles in combustion reactions, J. Solid State Chem. 219 (2014) 67–73.
[12] J.Y. Ahn, J.H. Kim, J.M. Kim, D.W. Lee, J.K. Park, D. Lee, S.H. Kim, Combustion characteristics of high-energy Al/CuO composite powders: the role of oxidizer structure and pellet density, Powder Technol. 241 (2013) 67–73.
[13] C. Rossi, K. Zhang, D. Esteve, P. Alphonse, P. Tailhades, C. Vahlas, Nanoenergetic materials for MEMS: a review, J. Microelectromech. Syst. 16 (4) (2007) 919–931.
[14] X. Zhou, M. Torabi, J. Lu, R. Shen, K. Zhang, Nanostructured energetic composites: synthesis, ignition/combustion modeling, and applications, ACS Appl. Mater. Interfaces 6 (5) (2014) 3058–3074.
[15] A.K. Sikder, N. Sikder, A review of advanced high performance, insensitive and thermally stable energetic materials emerging for military and space applications, J. Hazard. Mater. 112 (1–2) (2004) 1–15.
[16] K. Zhang, C. Rossi, M. Petrantoni, N. Mauran, A nano initiator realized by integrating Al/CuO-based nanoenergetic materials with a Au/Pt/Cr microheater, J. Microelectromech. Syst. 17 (4) (2008) 832–836.
[17] H. Liu, L. Zhang, K.H.H. Li, O.K. Tan, Microhotplates for metal oxide semiconductor gas sensor applications-towards the CMOS-MEMS monolithic approach, Micromachines 9 (11) (2018) 557.
[18] J. Wang, J. Yu, Multifunctional platform with CMOS-compatible tungsten microhotplate for pirani, temperature, and gas sensot, Micromachines 6 (11) (2015) 1597–1605.
[19] P.B. Butler, J. Kang, H. Krier, Modeling and numerical simulation of the internal thermochemistry of automotive airbag inflators, Prog. Energy Combust. Sci. 19 (1993) 365–382.
[20] E.F. Garner, S. Calif, Low temperature gas generator propellant, U.S. Patent No 3,912,562, October 14, 1975.

[21] G. Jian, J. Feng, R.J. Jacob, G.C. Egan, M.R. Zachariah, Super-reactive nanoenergetic gas generators based on periodate salts, Angew. Chem. Int. Ed. 52 (2013) 1–5.
[22] D.R. Poole, M.A. Wilson, Azide gas generating composition for inflatable devices, U.S. Patent No. 4,931,111, June 05, 1990.
[23] M.A. DiValentin, Metal oxide/azide gas generating compositions, U.S. Patent No. 3,996,079, December 07, 1976.
[24] C. Hock, M.P. Jordan, G.W. Pratt, A.J. Ward, Airbag inflator having a housing protected from high-temperature reactive generated gases, EP0733520B1, June 16, 1999.
[25] T.M. Klapötke, D.G. Piercey, 1, 1′-Azobis (tetrazole): a highly energetic nitrogen-rich compound with a N10 chain, Inorg. Chem. 50 (7) (2011) 2732–2734.
[26] D.E. Chavez, M.A. Hiskey, 1, 2, 4, 5-tetrazine based energetic materials, J. Energ. Mater. 17 (4) (1999) 357–377.
[27] P.S. Khandhadia, S.P. Burns, Thermally stable nonazide automotive airbag propellants, U.S. Patent 6, 306, 232, October 23, 2001.
[28] E. Gast, B. Schmid, C. Recker, S. Walz, T. Mayr, P. Semmler, Gas generator fuel composition, U.S. Patent No. 2004/0108031, June 10, 2004.
[29] T. Sugiyama, N. Itadzu, S. Nishi, Burning characteristics and sensitivity characteristics of some guanidinium 1, 5′-bis-1H-tetrazolate/metal oxide mixtures as candidate gas generating agent, Propell. Explos. Pyrotech. 36 (1) (2011) 51–56.
[30] S.P. Burns, P.S. Khandhadia, For inflating airbags and actuating seatbelt pretensioners in passenger-restraint devices, U.S. Patent No.6287400, 2001.
[31] G.K. Lund, M.R. Stevens, W.W. Edwards, G.C. Shaw, Non-azide gas generant formulation, method, and apparatus, U.S. Patent No. 5,197,758, March 30, 1993.
[32] D. Zhang, S. Lu, C.-Y. Cao, C.-C. Liu, L.-L. Gong, H.-P. Zhang, Impacts on combustion behavior of adding nanosized metal oxide to CH_3N_5-$Sr(NO_3)_2$ propellant, Fuel 191 (2017) 371–382.
[33] C. Wu, K. Sullivan, S. Chowdhury, G. Jian, L. Zhou, M.R. Zachariah, Encapsulation of perchlorate salts within metal oxides for application as nanoenergetic oxidizers, Adv. Funct. Mater. 22 (1) (2012) 78–85.
[34] G. Jian, J. Feng, R.J. Jacob, G.C. Egan, M.R. Zachariah, Super-reactive nanoenergetic gas generators based on periodate salts, Angew. Chem. Int. Ed. 52 (37) (2013) 9743–9746.
[35] W. Zhou, J.B. DeLisio, X. Li, L. Liu, M.R. Zachariah, Persulfate salt as an oxidizer for biocidal energetic nano-thermites, J. Mater. Chem. A 3 (22) (2015) 11838–11846.
[36] A. Eslami, S.G. Hosseini, V. Asadi, The effect of microencapsulation with nitrocellulose on thermal properties of sodium azide particles, Prog. Org. Coat. 65 (2) (2009) 269–274.
[37] H. Potvin, M.H. Back, A study of the decomposition of sodium azide using differential thermal analysis, Can. J. Chem. 51 (2) (1973) 183–186.
[38] K.S. Martirosyan, Nanoenergetic gas-generators: principles and applications, J. Mater. Chem. 21 (26) (2011) 9400–9405.
[39] L. Zhou, N. Piekiel, S. Chowdhury, M.R. Zachariah, Time-resolved mass spectrometry of the exothermic reaction between nanoaluminum and metal oxides: the role of oxygen release, J. Phys. Chem. C 114 (33) (2010) 14269–14275.
[40] C.E. Aumann, G.L. Skofronick, J.A. Martin, Oxidation behavior of aluminum nanopowders, J. Vac. Sci. Technol. B 13 (3) (1995) 1178–1183.
[41] L. Menon, S. Patibandla, K.B. Ram, S.I. Shkuratov, D. Aurongzeb, M. Holtz, H. Temkin, Ignition studies of Al/Fe_2O_3 energetic nanocomposites, Appl. Phys. Lett. 84 (23) (2004) 4735–4737.